Structure and Dynamics of Disodium Hydrogen 12-Tungstophosphoric Acid

Steven F. Dec*

Department of Chemistry and Geochemistry, Colorado School of Mines, Golden, Colorado 80401

Andrew M. Herring

Department of Chemical Engineering, Colorado School of Mines, Golden, Colorado 80401

Received: December 30, 2003; In Final Form: May 30, 2004

The structure and dynamics of the limiting hydrated form of disodium hydrogen 12-tungstophosphoric acid (HNaPW) were investigated as a function of temperature using solid-state ^{1}H, ^{23}Na, and ^{31}P nuclear magnetic resonance spectroscopy, infrared spectroscopy, and X-ray analysis. The ^{1}H nonspinning (NS) and magic-angle spinning (MAS) NMR results indicate that the limiting hydrated form of HNaPW has two types of protons. One type of proton corresponds to lone protons isolated from all other protons in the material. The second type of proton corresponds to an isolated proton pair of a water molecule. ^{1}H NS NMR spectra recorded from 168 to 393 K, in combination with theoretical simulations, show that the proton dynamics of the water molecule can be characterized by four temperature ranges above 168 K, the temperature corresponding to a rigid lattice. From 168 to 203 K, proton motion is minimal; from 203 to 293 K, the proton motion is dominated by rotational diffusion; from 293 to 383 K, both translational and rotational diffusion characterize the motion; above 383 K, the water molecule protons undergo chemical exchange with the lone protons of the material. The ^{23}Na NS and MAS NMR results, along with simulations of the spectra based on the second-order quadrupolar frequency shift, indicate that two six-coordinate sodium sites are present in this material. The six nearest neighbors of each sodium cation are oxygen atoms. $^{23}Na\{^{1}H\}$ spin−echo double-resonance (SEDOR) NMR and theoretical calculations show that sodium and proton sites are separated by at least 686 pm. The two sodium sites persist to temperatures near 383 K but the quadrupole coupling constant of each site decreases with temperature suggesting that the two sodium sites have increased mobility at higher temperature, possibly a result of lattice expansion. Results from ^{31}P NS and MAS NMR experiments show that there are three different four-coordinate phosphorus sites. The nearest neighbors of each phosphorus site are oxygen atoms and each phosphorus site has local tetrahedral symmetry. A $^{31}P\{^{1}H\}$ SEDOR experiment shows that all phosphorus sites are coupled to ^{1}H nuclei. Room-temperature $^{1}H\{^{31}P\}$ rotational echo double-resonance (REDOR) NMR experiments show that the lone proton and water molecule protons are both coupled to two phosphorus sites. Both of these types of protons are part of the secondary structure of the Keggin anion and are in relative motion to the two ^{31}P sites. Infrared results show that the lone proton asymmetrically bridges four terminal oxygen atoms of the Keggin anion and that the water molecule protons are hydrogen bonded to terminal oxygen atoms of the Keggin anion. X-ray analysis shows that the unit cell has cubic symmetry with a cell parameter $a = 1197$ pm. Elemental analysis along with the results of NMR experiments show that the formula of the limiting hydrated form of this commercially available salt should be written as $H_{0.5}Na_{2.5}PW_{12}O_{40}\cdot 4H_2O$.

Introduction

Proton-conducting membrane, PEM, fuel cells are an extremely attractive power source for a variety of applications from small portable devices to transportation and distributed power.[1] Although PEM fuel cells represent an attractive technology, there are still a large number of materials issues to be resolved associated with the high cost and low durability of these systems.[2,3] The major disadvantage of PEM fuel cells is the inability of the perfluorinated ionomer employed as the membrane to operate satisfactorily under conditions of low humidity and at temperatures above 373 K.[1,4] The typical operating temperature of a PEM fuel cell of 353 K necessitates the use of hydrogen with a very low CO content, less than a few ppm, and precludes combined heat and power applications because of the low quality of the waste heat. Operation of a fuel cell above 393 K would allow the use of hydrogen contaminated with some CO, reducing the complexity and hence expense of reforming hydrocarbon fuels into hydrogen. There is a need to develop new proton-conducting systems capable of operating at temperatures above 373 K and at reduced humidities. It is therefore important to develop a fundamental understanding of proton conduction in systems that are stable above 373 K and that do not need excessive humidification.

A large variety of proton-conducting solids are known.[3] Particularly attractive among these are the heteropoly acids (HPA) because these materials have high room-temperature proton conductivities and good thermal stabilities to temperatures above 625 K. Nafion shows a dramatic increase in fuel cell response when doped with HPA.[5,6] Several reports have appeared recently in which the HPAs have been incorporated

* Corresponding author. E-mail: sdec@mines.edu.

10.1021/jp038044s CCC: $27.50 © 2004 American Chemical Society
Published on Web 07/24/2004

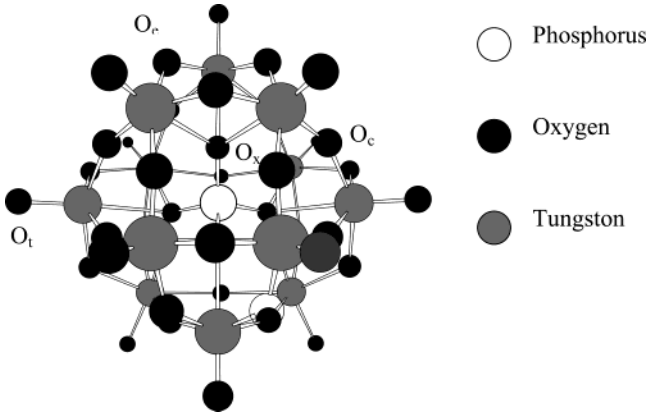

Figure 1. Schematic diagram of the $PW_{12}O_{40}^{3-}$ Keggin anion showing edge-sharing (O_e), corner-sharing (O_c), terminal (O_t), and phosphorus bound (O_x) oxygen atoms of the structure.

into a variety of membrane-ready substrates and their proton conductivities measured.[7−12]

The HPAs are composed of a heteroatom, which can be almost any atom in the periodic table, that is surrounded by several metal oxygen octahedra; the metal is usually tungsten or molybdenum or less commonly vanadium or uranium. The most widely available and studied HPAs are the Keggin anions. Of these, the most thoroughly studied are $H_3PW_{12}O_{40}$ (HPW) and $H_3PMo_{12}O_{40}$ (HPMo)[13−17] which consist of a centrally located, four-coordinate phosphorus linked via oxygen atoms to twelve tungston−oxygen and molebdenum−oxygen octahedra, respectively. A schematic diagram of the $PW_{12}O_{40}^{3-}$ anion is shown in Figure 1. These anionic structures form the so-called primary structure of these solids. The countercations are often protons and proton conduction is believed to occur in the space between the anions, often referred to as the secondary structure or pseudoliquid phase. Various other cations can substitute for some or all of the protons in HPAs. The effect of cation substitution and degree of hydration on proton conductivity has been investigated for several HPA salts[18] but the structural basis for the proton conductivity has largely been unexplored in these cases.

A single-crystal neutron diffraction study[15] confirmed the HPW hexahydrate, $H_3PW{\cdot}6H_2O$, (HPW in its high-temperature-limited hydration state) anionic cubic structure of Keggin and showed that all hydrogen atoms are present as $H_5O_2^+$. A quasielastic neutron diffraction scattering study[19] of $H_3PW{\cdot}6H_2O$ has shown that the water molecules in the $H_5O_2^+$ complex undergo a twofold reorientation about the central hydrogen bond. Attempts to measure the proton diffusion coefficient of $H_3PW{\cdot}6H_2O$ in the temperature range of 260−300 K were unsuccessful[20] even though the fully hydrated $HPW{\cdot}22H_2O$ exhibits a large proton conductivity.[3]

Multinuclear nuclear magnetic resonance (NMR), infrared (IR), and X-ray diffraction (XRD) studies of HPA materials potentially provide for understanding the structural basis for proton conductivity. Four ^{17}O resonance lines, corresponding to the four chemically distinct oxygen sites in the $PW_{12}O_{40}^{3-}$ anion, the so-called terminal (O_t), corner-sharing (O_c), and edge-sharing (O_e) oxygen atoms of the octahedra and the oxygen atoms of the tetrahedron (O_x), have been assigned using liquid-state ^{17}O NMR.[21,22] Solid-state ^{17}O magic-angle spinning (MAS) NMR resolved the three resonance lines due to the oxygen sites in the octahedra of the Keggin anions of HPW.[23] Deuterium wide-line spectra of HPW with hydration levels less than six water molecules are rather featureless indicating a disordered secondary structure.[24] Measurements of the ^{31}P spin−lattice relaxation time as a function of hydration level have been used to suggest that protons can either penetrate the Keggin anion or rapidly migrate among various Keggin anion surface sites.[25] The primary structure of HPAs have been fully characterized by IR spectroscopy[26] although many of these studies have involved salt pellets in which the secondary structure is expected to be partially or fully neutralized. The secondary structure of some HPAs have also been studied by IR using methods that leave the secondary structure intact.[27−29]

Solid-state ^1H and ^{31}P MAS NMR spectra obtained as a function of hydration level and temperature have revealed several distinct proton and phosphorus sites in HPW.[23,30,31] The 173 K ^{31}P MAS NMR spectrum of HPW containing about two water molecules exhibited four resonance lines that coalesced to a single peak at 298 K. A model based on the number of so-called isolated acidic protons per Keggin anion (0−3) was used to assign the resonance lines in the 173 K ^{31}P MAS NMR spectrum and to suggest that the protons in the secondary structure exist as both H_3O^+ and $H_5O_2^+$. The temperature dependence of the ^{31}P MAS NMR spectrum is also consistent with a 200 Hz proton chemical exchange rate among the Keggin anions.

On the basis of these and other studies, two types of waters of hydration may be identified: (a) those stable at low temperatures, that is, the waters of crystallization in which proton conduction can be described in terms of acidified water and is well understood[3] and (b) those stable at higher temperatures, that is, the waters of hydration in the secondary structure whose proton conduction will presumably be described on a case-by-case basis until structure−activity correlations can be developed. It is one goal of this study to broaden the base of understanding of proton conduction in HPAs that are or have been heated to temperatures above 373 K and therefore contain only secondary structural water at a particular temperature. It has been our observation that when heated to even higher temperatures, HPAs continue to lose waters from the secondary structure until they reach a limited hydration state, from which additional dehydration no longer occurs until the temperature is increased further, a process that often leads to the neutralization of the anion by loss of structural oxygen atoms with secondary structure protons as water.

In this work, solid-state NMR techniques, IR spectroscopy, and XRD are used to study the structure and dynamics of $HNa_2PW_{12}O_{40}$, the disodium salt of HPW, in its limiting hydrated form as a function of temperature. Solid-state MAS and nonspinning (NS) NMR spectra were recorded for ^1H, ^{23}Na, and ^{31}P. In addition, rotational echo double-resonance (REDOR)[32−35] and spin−echo double-resonance (SEDOR)[36−39] NMR experiments were performed for both $^1H-^{23}Na$ and $^1H-^{31}P$ spin pairs. The ^1H NS NMR spectra were analyzed using the theory developed by Nevzorov and Freed to calculate the line shape modulation from both rotational and translational diffusion for the case of a pair of like spins[40] and for a large bath of like spins.[41]

Experimental Section

Elemental Analysis. The elemental compostion of the commercially available HNaPW (Fluka, lot 90600) was obtained using inductively coupled plasma (ICP) analysis with a Perkin-Elmer Dual View ICP-AES. A 1% NH_4OH matrix was used. The following atomic ratios were obtained: W:P = 11.9 ± 1.0, W:Na = 4.6 ± 0.4, and Na:P = 2.5 ± 0.2.

Sample Preparation. The limiting hydrated form of HNaPW was obtained by heating the as-received material in air in an

oven at about 383 K for at least 17 days. For the NMR experiments, immediately prior to use, an amount of limiting hydrated HNaPW was removed from the oven and transferred to a glass NMR sample tube or magic-angle spinning (MAS) rotor. Samples were then heated in the NMR probe at 383 K for a least 0.5 h to remove any water that may have condensed onto the sample during the sample transfer process. For the IR experiments, about 200 mg of limiting hydrated HNaPW was loaded into a Harrick heatable variable atmosphere cell (HVAC) equipped with KBr windows.

NMR Experiments. All NMR spectra were recorded on a two-channel Chemagnetics CMX Infinity 400 NMR spectrometer operating at 400.0, 105.8, 161.8, and 83.4 MHz for ^{1}H, ^{23}Na, ^{31}P, and ^{207}Pb, respectively. Nonspinning ^{1}H NMR spectra were obtained on a home-built probe using 7-mm OD glass tubes (sample volume about 500 μL). All other NS and MAS ^{1}H, ^{23}Na, ^{31}P, and ^{207}Pb NMR spectra were obtained using a Chemagnetics 5-mm double-resonance, MAS probe equipped with a Pencil spinning module. This spectrometer is equipped with Chemagnetics solid-state variable temperature and speed controllers.

Chemical shift references, obtained by sample substitution, for ^{1}H, ^{23}Na, and ^{31}P were H_2O(l), NaCl(s), and 85% H_3PO_4, respectively, and were assigned chemical shift values of 4.8, 7.2, and 0 ppm, respectively, at 298 K. Therefore, the chemical shifts reported in this work for ^{1}H, ^{23}Na, and ^{31}P are relative to TMS, 1 M NaCl(aq), and 85% H_3PO_4, respectively. The ^{207}Pb chemical shift of $Pb(NO_3)_2$(s) was assigned a value of 0 ppm at a temperature of 298 K.

Nonspinning ^{1}H NMR spectra were recorded using 3.70-μs (90°) pulses and relaxation delays of 5 s. Because the Chemagnetics 5-mm probe has a large proton background signal from some of the probe materials, ^{1}H MAS NMR spectra were recorded using the DEPTH pulse sequence[42] with 4-μs (90° tip angle) pulses and 10-s relaxation delays. The ^{1}H T_1 value was determined to be less than 2 s at 310 K using a progressive saturation type pulse sequence.[43] ^{23}Na MAS NMR spectra were recorded using single-pulse excitation with 0.50 μs pulses (13.5° tip angle for the $m = {}^1/_2 \leftrightarrow -{}^1/_2$ transition[44] of this I = 3/2 nuclide) and relaxation delays of 2 s; spectra were recorded both with and without proton decoupling (50 kHz) during acquisition. ^{31}P MAS NMR spectra were recorded using single-pulse excitation with 3.50-μs pulses (90° tip angle) and relaxation delays of 900 s; spectra were recorded both with and without proton decoupling (50 kHz) during acquisition. The ^{31}P T_1 was 175 s at 310 K using a progressive saturation type experiment.[43] All ^{1}H, ^{23}Na, and ^{31}P MAS NMR spectra were recorded using an MAS speed of 10.0 kHz unless otherwise noted. The maximum MAS speed was limited to 10 kHz because the manufacturer's maximum speed rating is 12 kHz for 2 g ml^{-1} density samples for the 5-mm zirconia rotor and the limiting hydrated form of HNaPW has a density of about 5 g ml^{-1}. As will be shown below, all resonance lines for all nuclei observed in this study are inhomogeneously broadened and therefore the resolution of all isotopic peaks is essentially independent of MAS speed. The pulse sequence used to obtain the REDOR NMR spectra is shown in Figure 2.[33]

Temperature calibration of the nonspinning, home-built probe was performed by measuring the ^{1}H chemical shift separation of the two proton resonance lines in methanol[45] for temperatures less than or equal to 298 K and ethylene glycol[46] for temperatures above 298 K. Temperature calibration of the 5-mm MAS probe was performed by first measuring the ^{1}H chemical shift separation of the two resonance lines in methanol near room temperature and then assigning the ^{207}Pb isotropic chemical shift of $Pb(NO_3)_2$(s), as determined in a ^{207}Pb MAS NMR experiment, to reflect this temperature.[47] Care was taken to extrapolate the ^{207}Pb chemical shift of $Pb(NO_3)_2$ to zero MAS speed to account for frictional heating due to sample spinning[47] that was found to have the following effect on the ^{207}Pb isotropic chemical shift:

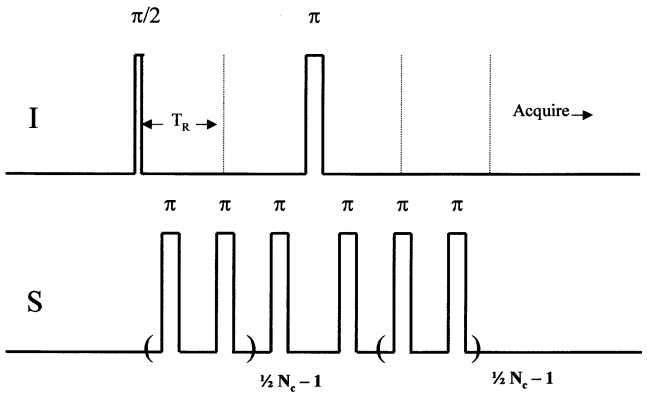

Figure 2. REDOR pulse sequence. I corresponds to the observed nucleus (^{1}H or ^{31}P) and the π dephasing pulses are applied to the S nucleus (^{31}P or ^{1}H).

$$\delta(\nu_R) = 0.1085\nu_R^2 - 0.2002\nu_R + 0.0795 \quad (1)$$

$\delta(\nu_R)$ is the isotropic chemical shift (ppm) at rotational frequency ν_R (kHz) in the frequency range of 1.25−10.0 kHz. The probe temperature for higher temperatures was determined by measuring the ^{207}Pb chemical shift of $Pb(NO_3)_2$ using the expression[47]

$$\delta(t_2) - \delta(t_1) = 0.735(t_2 - t_1) \quad (2)$$

where $\delta(t_i)$ is the chemical shift at temperature t_i. The variation of the ^{207}Pb isotropic chemical shift of $Pb(NO_3)_2$(s) varied linearly with temperature between 310 and 410 K at 10.0 kHz MAS.

Infrared Spectroscopy. Infrared spectra were recorded with a Thermo-Nicolet Nexus 670 FT infrared spectrometer. Diffuse reflectance infrared Fourier transform spectroscopy (DRIFTS) spectra were recorded in a Harrick heatable, variable atmosphere cell (HVAC) using a Harrick Praying Mantis diffuse reflectance attachment (DRA) under an atmosphere of dry helium. Samples aged in the oven were pretreated at 425 K for 20 min to drive off any water that the sample may have absorbed during transfer from the oven to the HVAC.

X-ray Diffraction. X-ray powder patterns were recorded using a Rigaku diffractometer with a CuKα radiation source. A range of 5−65° was scanned using a 0.02° s^{-1} step size. The cubic lattice parameters were returned using a least-squares method.[48]

Simulations. All simulations were performed using MATLAB[49] based code. The code used to calculate the effect of rotational and translational diffusion on the ^{1}H NS NMR spectra of the limiting hydrated form of HNaPW is based on the expressions developed by Nevzorov and Freed.[40] The calculated spectra are strong functions of the diffusion coefficient, D, the rigid lattice interproton distance, d, and a maximum interproton distance, r_{max}. The calculated line shapes were convoluted with a Lorentzian function with line broadening of 1.5 kHz.

For computational convenience, the line shape function used in all other simulations was a Lorentzian function[50] with line broadening of a few kHz. The expression of Zilm and Grant[51] was used to calculate the line shape for ^{1}H NS NMR spectra that have contributions from both homonuclear dipole and

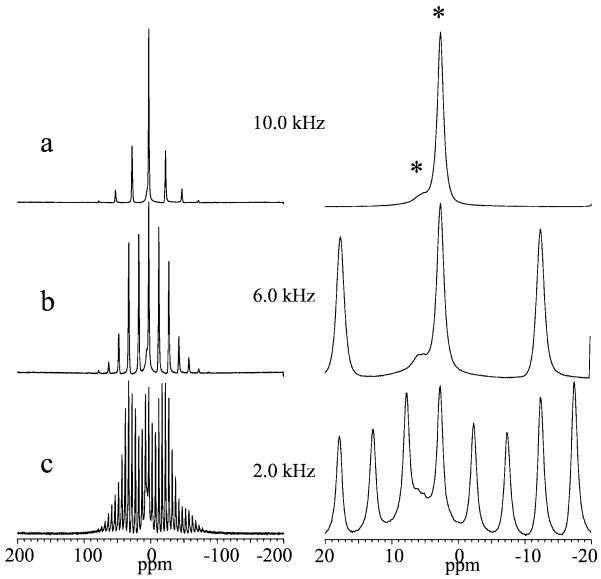

Figure 3. 400 MHz ^{1}H MAS NMR spectra of the limiting hydrated form of HNaPW, (a) 10.0 kHz MAS and $T = 310$ K, (b) 6.0 kHz MAS and $T = 302$ K and (c) 2.0 kHz MAS and $T = 298$ K. An * denotes the isotropic peak; all other peaks are spinning sidebands.

chemical shift effects. The line shape for a triangular cluster of protons was calculated using the expressions of Andrew and Bersohn.[52] The line shape for the $m = {}^1/_2 \leftrightarrow -{}^1/_2$ transition of ^{23}Na (spin I = 3/2) NS spectra was calculated using the expression for the second-order quadrupolar frequency shift.[53]

Results and Discussion.

^{1}H NMR. Figure 1S shows nonspinning ^{1}H NS NMR spectra of the limiting hydrated form of HNaPW as a function of temperature between 168 and 393 K. As will be discussed in detail below, the temperature dependence is primarily due to an increase in proton diffusion as the temperature increases and the 168 K spectrum corresponds to the rigid lattice. The complex line shape exhibited in all spectra can only be due to a limited number of possible proton structures in this system. The most likely structures are lone protons, protons in a H_2O molecule, and protons in a H_3O^+ molecule. Clusters of four or more protons exhibit featureless ^{1}H NS NMR spectral line shapes.[54] More specific structural assignments can be made with the aid of ^{1}H MAS NMR spectra of this material.

Figure 3 shows ^{1}H MAS NMR spectra of the limiting hydrated form of HNaPW as a function of MAS speed near 310 K. The spectra exhibit MAS sideband patterns characteristic of an inhomogeneously broadened line,[55] that is, a narrow centerband and spinning sidebands are observed even at 2.0 kHz MAS, Figure 3c. Upon increasing the MAS speed to 10.0 kHz, Figure 3a, no additional narrowing of the centerband is obtained; only the number and frequency position of the spinning sidebands changes. Closer inspection of the centerband region of the ^{1}H MAS NMR spectrum shows the presence of two isotropic regions, the peak giving rise to the spinning sideband array at 2.7 ppm and a shoulder centered at about 5.8 ppm. The ^{1}H MAS NMR spectra show that no spinning sideband intensity attributable to the resonance intensity at 5.8 ppm is present at any MAS speed. Hence, any dipolar coupling to these types of protons must be much less than 2.0 kHz near 310 K. The resonance intensity at about 5.8 ppm is actually composed of two resonance lines that are barely apparent at 10.0 kHz MAS but more clearly observed at lower MAS speeds. These two resonance lines will be collectively called the 5.8 ppm peak throughout the remainder of this work.

The behavior of the two isotropic peaks at 2.7 and 5.8 ppm as a function of MAS speed virtually eliminates H_3O^+ as a possible structure in the limiting hydrated form of HNaPW. The ^{1}H MAS NMR spectrum of H_3O^+ would yield a spinning sideband pattern characteristic of a homogeneously broadened line,[55] that is, one where the centerband narrows as the MAS speed increases. More evidence eliminating the H_3O^+ structure is provided in Figure 2S where simulations of the powder pattern expected for an equilateral triangular configuration of protons,[52] as in H_3O^+, are compared with the experimental 168 K ^{1}H NS NMR spectrum. Figure 2Sb is a simulation using an interproton distance of 172 pm typically found for H_3O^+ in solid monohydrates of nitric, perchloric, and sulfuric acids.[56] The separation of the outer maxima in this case is about 56 kHz, much greater than the observed separation of 42 kHz of the two most intense maxima of the 168 K experimental spectrum, Figures 1S and 2Sa. Figure 2Sc shows a simulation using an unrealistically large interproton distance of 200 pm for the equilateral triangular configuration of protons. In this case, the separation of the outer maxima is 38 kHz but the agreement of theoretical and experimental line shapes is again extremely poor.

The ^{1}H MAS NMR spectra of Figure 3 also suggest that the relatively sharp resonance line with a chemical shift of about 5 ppm observed in the ^{1}H NS NMR spectra of Figure 1S is due to protons that are either in isolated or highly mobile sites because there are no spinning sidebands associated with the ^{1}H MAS NMR 5.8 ppm resonance line. Therefore, the dominant feature of the ^{1}H NS NMR spectra with resonance intensity from about 80 to -80 ppm is most likely due to an isolated pair of protons, that is, a Pake doublet.[57]

The temperature dependence of the nonspinning ^{1}H NMR spectra of Figure 1S is now discussed in more detail. As the temperature is increased from 293 to 343 K, the separation of the horns of the Pake doublet is clearly observed to decrease. Minimal change is observed in the appearance of the lone proton peak. Above 343 K, the Pake doublet is observed to progressively narrow until at 383 K it has virtually disappeared.

As the temperature is decreased below 293 K, the lone proton peak is observed to broaden. Dipolar interactions with other protons are probably not responsible for the observed broadening because the Pake pattern remains well-defined at low temperatures; additional proton dipolar coupling to the protons responsible for the Pake doublet would result in protons behaving homogeneously[55] and a broad featureless line shape would be expected. Dipolar coupling of the protons to the ^{23}Na nuclei present in this system are also probably not responsible for the observed broadening because these dipolar interactions are negligibly small (see below). In contrast, dipolar coupling of the protons to the ^{31}P nuclei should make a significant contribution (see below). Line broadening of the lone proton resonance line probably also has contributions from freezing-in of disorder of the protons as the temperature is decreased. Disorder leads to a variety of slightly different chemical environments for the lone protons that results in a dispersion of chemical shifts, yielding a broader resonance line.

The Pake doublet is also observed to broaden as the temperature is decreased from 293 to 168 K. This is more clearly seen in a plot of the apparent dipolar coupling frequency, $\nu_{D,app}$, versus temperature, Figure 3S. For the purposes of this discussion, $\nu_{D,app}$ is defined as two-thirds of the frequency separation of the horns of the Pake doublet. Figure 3S shows that $\nu_{D,app}$ approaches an asymptotic value as the temperature

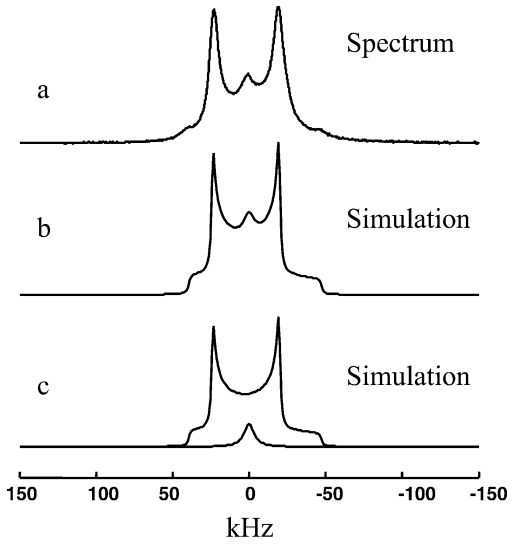

Figure 4. 400 MHz ^{1}H NS NMR spectra of the limiting hydrated form of HNaPW at 168 K. (a) Spectrum (b) simulation of proton pair separated by 161.4 pm and (c) two individual components of simulation in b.

is decreased to 168 K, the lowest temperature that can be reached with our current instrumentation. While an additional increase in $\nu_{D,app}$ might occur as the temperature is decreased below 168 K, the plot in Figure 3S suggests that such an increase in $\nu_{D,app}$ will be small. Thus, the spectrum recorded at 168 K corresponds closely to the one that would be obtained for a rigid lattice. For a rigid lattice[35]

$$\nu_{D,app} = \nu_D = \frac{h}{4\pi^2}\frac{\gamma_H^2}{r^3} \qquad (3)$$

where ν_D is the dipolar coupling frequency in hertz, h is Plank's constant, γ_H is the proton gyromagnetic ratio, and r is the interproton distance.

The 168 K ^{1}H NS NMR spectrum is shown in Figure 4a, along with a simulation of the spectrum, Figure 4b and 4c. The lone proton peak at the center of the spectrum is simulated using a single Lorentzian line contributing 6% of the total intensity, a result that is consistent with the ^{1}H MAS NMR results. The pattern observed in the ^{1}H NS NMR spectrum also suggests that the protons of the Pake doublet have an axially symmetric chemical shift tensor[58] similar to that observed for the protons in polycrystalline ice.[59,60] Zilm and Grant[51] give theoretical expressions for a powder line shape subject to both chemical shift and dipolar interactions. A good fit of the 168 K ^{1}H NS NMR spectrum is obtained for $\nu_D = 30$ kHz, a chemical shift anisotropy of 10.0 ppm, and a chemical shift asymmetry parameter of 0.0. The polar angle that relates the principal axes of the dipolar and chemical shift interaction tensors was 0° while the dependence of the simulation was virtually independent of the azimuthal angle. The value $\nu_D = 30$ kHz yields an interproton distance of 161.4 pm.[61] This value of ν_D is in the range observed by Pake[57] for the interproton distance of the water molecules in $CaSO_4 \cdot 2H_2O$ and other minerals. The *z*-axis of the dipole tensor principal axis system necessarily lies along the interproton vector connecting the two dipoles. A polar angle of 0° relating the dipole and chemical shift tensor principal axes for an axially symmetric chemical shift tensor corresponds to a *z*-axis of the chemical shift tensor principal axis system that is coplanar with the *z*-axis of the dipole tensor principal axis system. The protons of a water molecule have these relative

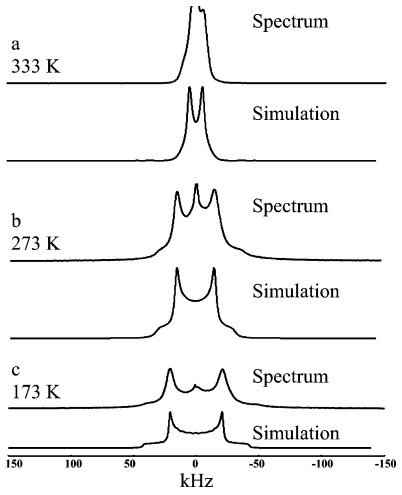

Figure 5. 400 MHz ^{1}H NS NMR spectra of the limiting hydrated form of HNaPW. (a) $T = 333$ K. Top: spectrum. Bottom: simulation. (b) $T = 273$ K. Top: spectrum. Bottom: simulation. (c) $T = 173$ K. Top: spectrum. Bottom: simulation. Simulations based on expressions in ref 40.

TABLE 1: Chemical Shifts and Relative Intensities of ^{1}H Resonance Lines Appearing in Figure 3

peak (ppm)	relative intensity (%)
5.8	5.5
2.7	47.2
spinning sidebands	47.3

orientations of the dipolar and chemical shift tensors. Thus, on the basis of the value of the interproton distance and the dipolar and chemical shift tensor relative orientations, the protons of the Pake doublet are assigned to protons of a water molecule.

Closer inspection of the ^{1}H NS NMR spectra of Figure 1S suggests the existence of four different temperature ranges where the proton dynamics exhibit a characteristic behavior. These are temperature ranges of 168−203, 203−293, 293−383, and 383−393 K. This observation can be put in more quantitative terms by considering the results of simulations based on the theory of Nevzorov and Freed.[40] Simulations of ^{1}H NS NMR spectra at 173, 273, and 333 K are shown in Figure 5. Results for the other temperatures between 168 and 393 K are similar. Values of the diffusion coefficient, D, and r_{max}/d as a function of temperature are listed in Table 1S and plotted in Figure 6.

Between 168 and 203 K, $r_{max}/d \approx 1$ and D is virtually constant at about 5×10^{-15} cm^2 s^{-1}. From 203 to 293 K, r_{max}/d and D gradually increase to 1.25 and 125×10^{-15} cm^2 s^{-1}, respectively. A value of r_{max}/d near unity indicates that the increase of D is primarily due to an increase of rotational diffusion of the proton pair.[40] Above 293 K, both r_{max}/d and D increase much more rapidly to $r_{max}/d \approx 2$ and $D \approx 4 \times 10^{-12}$ cm^2 s^{-1}, respectively, at 393 K. This more rapidly increasing value of r_{max}/d above 293 K indicates that translational diffusion of the protons in the proton pair becomes much more significant at these higher temperatures.[40]

The plot of ln(D) versus 1/T, Figure 6a, is highly nonlinear, suggesting that several physical processes are involved. Subsets of the data can be fit to an Arrhenius-type expression:

$$\ln(D) = \ln(D_0) - \frac{E_a}{RT} \qquad (4)$$

D_0 is a constant, E_a is the activation energy, and R is the gas constant. A fit of the ln(D) values for the six temperatures 203−253 K to eq 4 yields $E_a = 20$ kJ mol^{-1}, about the value of one

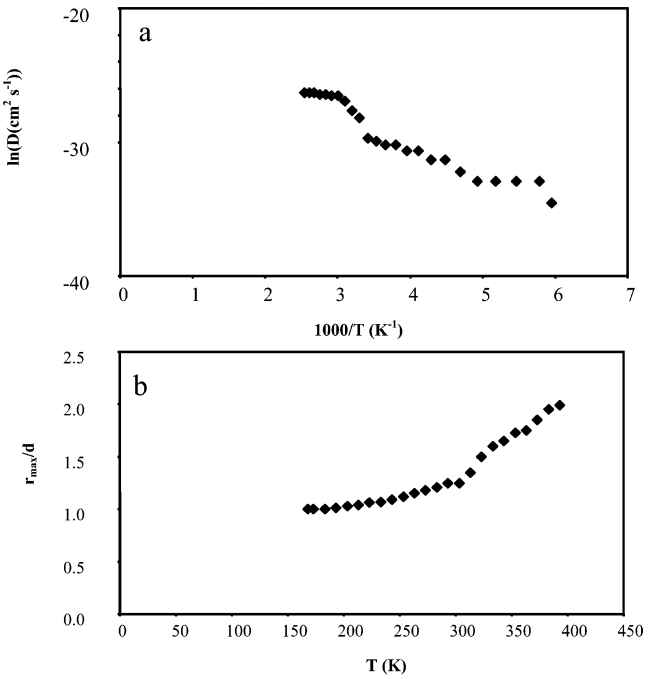

Figure 6. (a) Plot of ln(D) versus 1/T. (b) Plot of r_{max}/d versus T.

hydrogen bond in ice.[62] A fit of the ln(D) values for the five temperatures 293−333 K to eq 4 yields $E_a = 62$ kJ mol^{-1}, about twice the value of one hydrogen bond in ice. Thus, the onset of rotational diffusion of the water molecule near 203 K requires breaking one hydrogen bond whereas near 293 K, where translational and rotational diffusion both occur, two hydrogen bonds must be broken.

Above 383 K, the Pake doublet and lone proton resonance lines have coalesced indicating that chemical exchange between the two sites is occurring. Attempts to analyze the ^{1}H NS NMR spectra at 383 and 393 K using the expression for chemical exchange based on the Bloch equations[63] failed because the concentration of lone protons in the material is too small to have an effect on the overall line width. However, a simulation of the 393 K spectrum shown in Figure 4S, using the experimental line width of 4 kHz and the 200 Hz proton exchange rate observed by Misono and co-workers,[23] yields average lifetimes of 4 and 73 ms for the lone and water molecule protons sites, respectively.

Additional evidence for chemical exchange of the two types of protons in this system is provided by the ^{1}H MAS NMR spectra recorded at 310 and 384 K, shown in Figure 7. The centerband region of the ^{1}H MAS NMR spectrum at 384 K, Figure 7d, shows the presence of only one peak with an intensity maximum of 2.9 ppm. In the limit of fast chemical exchange between two sites A and B, the average chemical shift, δ_{ave}, is given by[64]

$$\delta_{ave} = p_A\delta_A + p_B\delta_B \qquad (5)$$

where p_i and δ_i are the fractional population and chemical shift of nuclei in site i, respectively. Substituting the p_i values listed in Table 1 into eq 5 yields $\delta_{ave} = 2.9$ ppm, in agreement with the observed value. Thus, the ^{1}H MAS NMR results are consistent with the ^{1}H NS NMR results and indicate that lone protons and water molecule protons in the limiting hydrated form of HNaPW undergo chemical exchange at elevated temperatures.

In addition, the ^{1}H MAS NMR spectrum recorded at 384 K, Figure 7, shows that the sideband intensity is severely attenuated, indicating a decrease in dipolar coupling of the water protons at this temperature. However, the sideband intensity makes a nonnegligible contribution to the total intensity of the spectrum even at 384 K indicating the persistence of dipolar coupling at this elevated temperature.

^{23}Na NMR. The ^{23}Na nucleus was studied using both NS and MAS techniques. As shown in Figure 5S, ^{1}H decoupling (50 kHz) had no effect on the appearance of the ^{23}Na NS NMR spectrum at 298 K. Hence, all other ^{23}Na NMR spectra shown in this work were recorded without ^{1}H decoupling. Figure 8a and 8b shows ^{23}Na MAS NMR spectra for the limiting hydrated form of HNaPW at 310 and 394 K, respectively. The intensity maximum of the 310 K spectrum has a peak position of −28.0 ppm. The shoulder at high-shielding values observed in the 310 K spectrum may indicate the presence of at least two different sodium sites. However, complex line shapes such as that observed in Figure 8a for the $m = {}^1/_2 \leftrightarrow -{}^1/_2$ transition of half-integer spin nuclei such as ^{23}Na (spin I = 3/2) can also be MAS-averaged second-order quadrupolar powder patterns.[65,66] Increasing the temperature to 394 K, Figure 8b, yields a more symmetrical line shape with an intensity maximum that shifts to a slightly higher frequency of −24.7 ppm relative to the 310 K spectrum. Some additional progress can be made by considering the ^{23}Na NS NMR spectra recorded at 298 and 394 K, shown in Figure 8c and 8d, respectively. Attempts to simulate the ^{23}Na NS NMR spectra using only a single sodium site yielded poor fits for all values of the quadrupole coupling constant, C_q, and asymmetry parameter, η, indicating that at least two different sodium sites are present in the limiting hydrated form of HNaPW. A two-site simulation of the 298 K ^{23}Na NS NMR spectrum is shown in Figure 6Sb and 6Sc and the results of the simulations at both 298 and 394 K are given in Table 2. The simulations are tentative at best; more definitive structural assignments await field-dependent or multiple-quantum MAS studies. However, all the ^{23}Na MAS NMR spectral intensity lies in the chemical shift range for sodium with a coordination number of six. Hence, the two unique sodium sites in the limiting hydrated form of HNaPW correspond to a sodium coordination number of six.[66]

In this system, the simplest likely structures for a six-coordinate sodium site that has axial symmetry ($\eta = 0$) are structures such as MAB_5 and MA_2B_4 [67] where M = Na and A and B are different ligands coordinated to M via oxygen atoms. For example, an MA_2B_4 structure would be one where Na is strongly coordinated to four corner oxygen atoms of a Keggin anion and more weakly coordinated to two other oxygen atoms in the structure. Similarly, for a six-coordinate sodium site with $\eta = 1.0$, the simplest likely structure in this system is MA_3B_3.[67] The fact that ^{1}H decoupling has no effect on the appearance of the ^{23}Na NS NMR spectrum indicates that the following type of structures are not present in the limiting hydrated form of HNaPW:

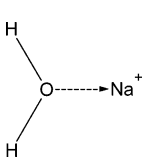

Additional insight regarding the location of the protons in this system relative to the sodium cations can be inferred from a comparison of a ^{23}Na{^{1}H} SEDOR experiment and theoretical calculations. The SEDOR fraction, $\Delta S/S_0 = (S_0 - S)/S_0$, is defined as the difference between the intensity of the ^{23}Na NS NMR resonance line obtained both with (S) and without (S_0)

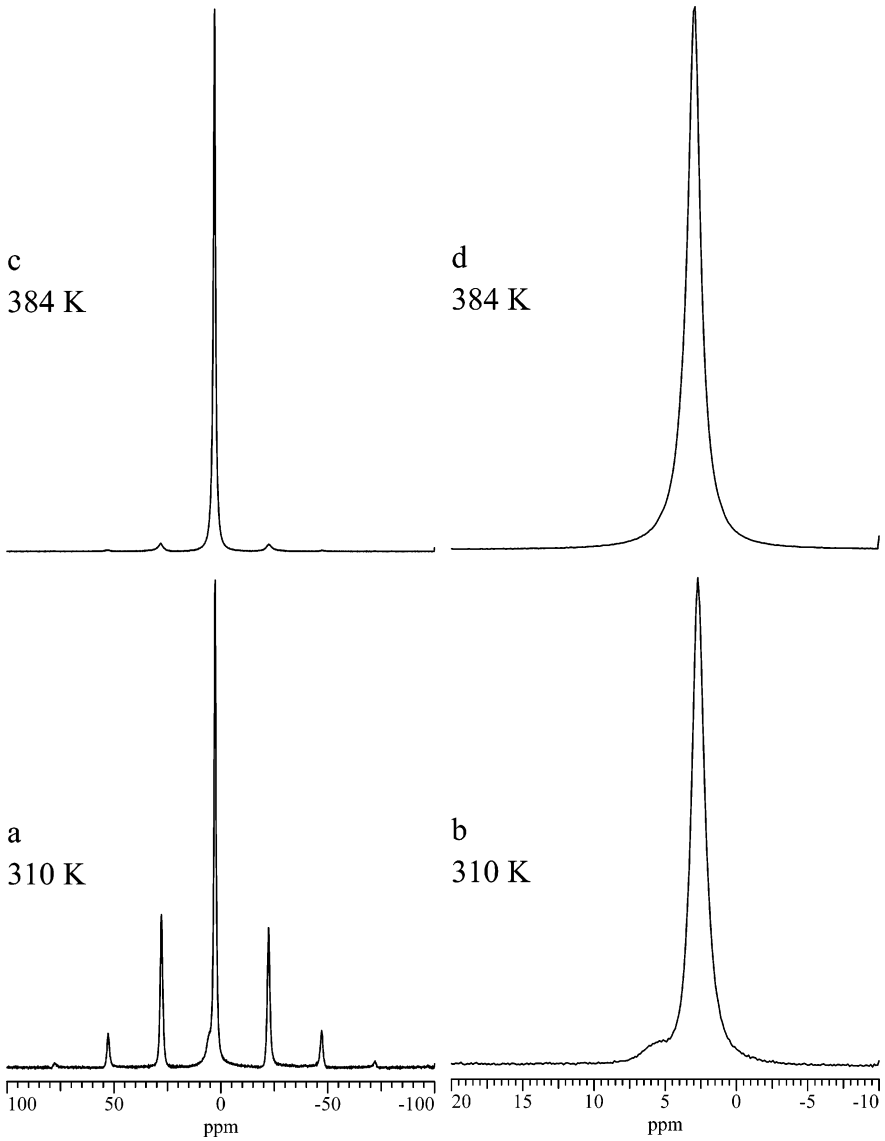

Figure 7. 400 MHz ^{1}H MAS NMR spectra of the limiting hydrated form of HNaPW at 10 kHz MAS. (a) and (b) $T = 310$ K, (c) and (d) $T = 384$ K.

^{1}H dephasing π-pulses divided by the intensity of the ^{23}Na NS NMR spectrum without (S_0) ^{1}H dephasing π-pulses. The SEDOR fraction signal intensity for one ^{23}Na$-^1$H spin pair is given by[39]

$$\frac{S_o - S}{S_o} = \alpha\langle 1 - \cos(2\pi\nu_D\tau)\rangle \qquad (6)$$

where α is a constant close to unity and τ is the time between the ^{23}Na $\pi/2$-pulse and ^{1}H π-pulse. The triangular brackets denote an average over all orientations. For ^{23}Na and ^{1}H nuclei that have a dipole interaction, the SEDOR fraction approaches an asymptotic value that is proportional to the fraction of ^{23}Na nuclei coupled to ^{1}H nuclei. If ^{23}Na and ^{1}H are not coupled to each other, the ^{1}H dephasing π-pulses make no difference and the SEDOR fraction is zero. The ^{23}Na{^{1}H} SEDOR results obtained at 298 K for the limiting hydrated form of HNaPW are shown in Figure 7S. The SEDOR fraction is zero for all values of τ used in the experiment. In addition, Figure 7Sa shows theoretical curves for ^{23}Na dipolar coupled to a lone proton while Figure 7Sb shows theoretical curves for ^{23}Na dipolar coupled to two rapidly rotating protons in a water molecule; theoretical curves for both models were obtained as a function of the ^{23}Na $-^1$H dipolar coupling frequency. The theoretical curves for both models indicate that the sodium-proton internuclear distance in the limiting hydrated form of HNaPW is at least 686 pm.[61]

Both the ^{23}Na NS and MAS NMR spectra of the limiting hydrated form of HNaPW narrow as the temperature is increased. This is readily seen by the decrease in C_q values determined for both sodium sites at higher temperatures, Table 2. The lack of sodium-proton coupling observed in the SEDOR experiment suggests that an effect other than increased proton motion at higher temperatures is the cause of the narrowing in the ^{23}Na NMR spectra; increased sodium cation mobility due to lattice expansion at elevated temperatures may be the source of the observed line narrowing in this case.

^{31}P NMR. In contrast to the ^{23}Na NS NMR spectra, the ^{31}P NS NMR spectra show significant line narrowing when ^{1}H decoupling is used. Measured line widths obtained with and without ^{1}H dcoupling are summarized in Table 3. With no ^{1}H decoupling, increasing the temperature from about 298 to 393 K decreases the ^{31}P NS line width by about 360 Hz, a result that is consistent with increased proton mobility at higher temperatures. The small but significant decrease in line width as the temperature is increased from 298 to 393 K when ^{1}H decoupling is used is consistent with the ^{23}Na results, that is,

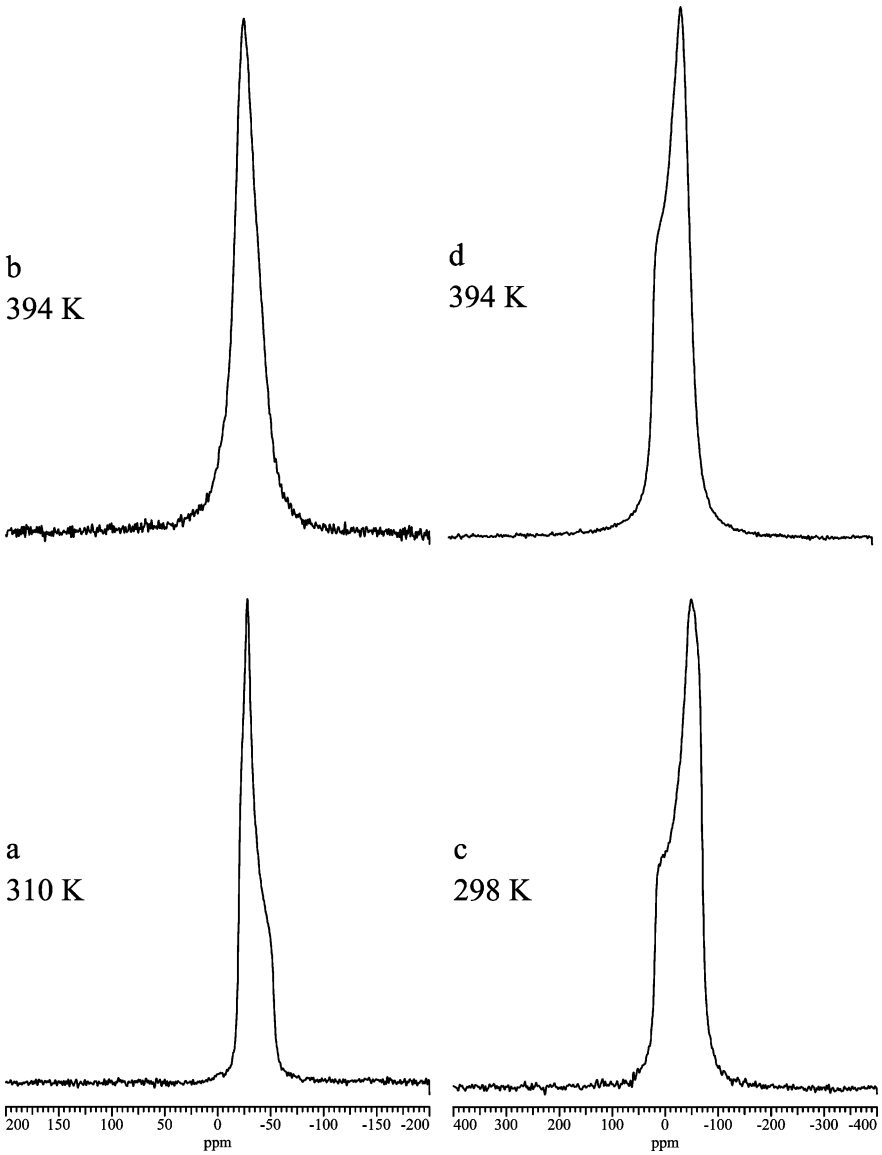

Figure 8. 105.8 MHz ^{23}Na NS and MAS NMR spectra of the limiting hydrated form of HNaPW as a function of temperature. (a) and (b), MAS spectra at 310 and 394 K, respectively. MAS speed was 10.0 kHz. (c) and (d), NS spectra at 298 and 394 K, respectively.

TABLE 2: ^{23}Na Isotropic Chemical Shifts, Quadrupole Coupling Constants, and Asymmetry Parameters of the Spectra Shown in Figure 8c and 8d

δ_{iso} (ppm)[a]	C_q (MHz)[a,b]	η[a,c]
	$T = 298$ K	
3	2.0	1.0
4	2.7	0.0
	$T = 394$ K	
3	1.8	1.0
7	2.3	0.0

[a] From simulation of spectra, ref 53. [b] $C_q = e^2qQ/h$ where e is the charge of an electron, Q is the quadrupole moment, and eq $= V_{zz}$ is the zz-component of the electric field gradient tensor, ref 53. [c] $\eta = (V_{xx} - V_{yy})/V_{zz}$ where the V_{ii} are the ii-components of the electric field gradient tensor, ref 53.

lattice expansion leads to increased sodium cation mobility that would also decouple ^{23}Na and ^{31}P nuclei.

Figure 8S shows ^{31}P MAS NMR spectra for the limiting hydrated form of HNaPW obtained at 310 and 405 K. ^{31}P MAS NMR spectra recorded both with proton decoupling (50 kHz) and without proton decoupling showed similar resolution. Hence, all ^{31}P MAS NMR spectra reported in this work were recorded without ^{1}H decoupling. At 310 K, the spectrum is dominated by a resonance line with a chemical shift at −15.4 ppm. Two high-frequency shoulders, with chemical shifts of −15.2 and −15.0 ppm, are also observed. The ^{31}P MAS NMR spectrum at 405 K has the same general appearance as that at 310 K but all three resonance lines have shifted to slightly lower shielding values. At 405 K, the most intense feature has a chemical shift of −15.2 ppm while the high-frequency shoulders have chemical shifts of −15.1 and −14.9 ppm. Chemical shift values and relative intensities of each resonance line are summarized in Table 4.

TABLE 3: ^{31}P NS NMR Line Widths (Hz) as a Function of Temperature Both with and without ^{1}H Decoupling of 50 kHz

T (K)	no ^{1}H-decoupling	with ^{1}H-decoupling
$T = 298$	950	370
$T = 393$	590	330

The three resonance lines observed in the ^{31}P MAS NMR spectra must correspond to four-coordinate phosphorus sites in the bulk material. In contrast to the dramatic changes observed in both the ^{1}H NS and MAS NMR spectra as the temperature is increased, the ^{31}P MAS NMR spectrum is essentially the same

TABLE 4: ^{31}P Chemical Shifts and Relative Intensities of the Spectra Shown in Figure 8S

peak (ppm)	relative intensity (%)[a]
$T = 310$ K	
−15.0	8.2
−15.2	24.3
−15.4	67.5
$T = 405$ K	
−14.9	9.6
−15.1	16.1
−15.2	74.3

[a] From deconvolution analysis of spectra.

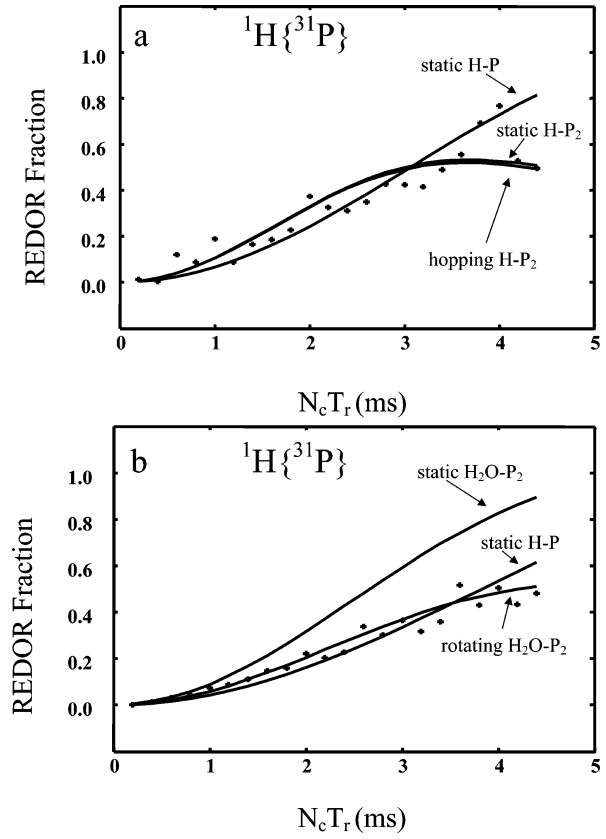

Figure 9. Plot of ^{1}H{^{31}P} REDOR fraction versus N_cT_r at 310 K and 10.0 kHz MAS. (a) 5.8 ppm ^{1}H peak, (b) 2.7 ppm ^{1}H peak.

at both 310 and 405 K. Hence, a change in the number of isolated acidic protons as shown by Misono and co-workers[23] to analyze the temperature of ^{31}P MAS NMR spectra of HPW does not explain the temperature dependence of ^{31}P MAS NMR spectra shown in Figure 8S. On the NMR time scale, the structure of the phosphorus sites in the limiting hydrated form of HNaPW at both 310 and 405 K are about the same.

The results of a set of ^{31}P{^{1}H} SEDOR NMR experiments for the limiting hydrated form of HNaPW are shown in Figure 9S. In contrast to the ^{23}Na{^{1}H} SEDOR NMR experiment, all phosphorus nuclei in this sample are coupled to protons because the value of the SEDOR fraction is about 1.0 for long values of τ.[36−39]

^{1}H{^{31}P} and ^{31}P{^{1}H} REDOR. To further investigate the nature of the proton and phosphorus structures in the limiting hydrated form of HNaPW, REDOR NMR experiments were performed. REDOR NMR can be used to determine intermolecular distances up to about 1500 pm when ^{1}H is one of the nuclei in the spin pair.[68] We discuss the ^{1}H{^{31}P} REDOR NMR results first because, as will become evident, modeling of the results of the ^{1}H{^{31}P} REDOR NMR experiment is more straightforward than that of the ^{31}P{^{1}H} REDOR NMR experiment.

Figure 9a and 9b shows plots of the ^{1}H{^{31}P} REDOR fraction versus N_cT_r for the limiting hydrated form of HNaPW at 310 K for the 5.8 and 2.7 ppm resonance lines, respectively, of the ^{1}H MAS NMR spectra of Figure 3. The REDOR pulse sequence is shown in Figure 2 and the experimental REDOR fraction is defined in the same way as the experimental SEDOR fraction (see above).

The models used to calculate theoretical REDOR curves have been derived by Goetz and Schaefer[35] and are summarized here. For an isolated, static I−S spin pair, the REDOR fraction is given by[35]

$$\Delta S = \frac{S_o - S}{S_o} = 1 - \frac{1}{4\pi}\int_{\alpha=0}^{2\pi}\int_{\beta=0}^{\pi} \times \cos[2\sqrt{2}\nu_D N_c T_R \sin(2\beta)\sin(\alpha)]d\alpha\sin(\beta)d\beta \quad (7)$$

N_c is the number of rotor cycles, T_R is the rotor period, and α, β are angles that describe the orientation of the ^{1}H−^{31}P internuclear vector relative to the rotor axis. The dipolar coupling frequency ν_D is defined in eq 3 with γ_H^2 replaced by $\gamma_I\gamma_S$ where γ_I and γ_S are the gyromagnetic ratios of spins I and S, respectively. For a single, static I-spin coupled to N different S-spins, the REDOR fraction becomes[35]

$$\Delta S = 1 - \frac{1}{8\pi^2}\int d\Omega \prod_{i=1}^{N}\cos[2\sqrt{2}\nu_D{}^i N_c T_R \sin(2\beta^i)\sin(\alpha^i)] \quad (8)$$

N is the total number of I−S dipolar couplings and dΩ[69] is the element of solid angle for powder averaging. For a single I-spin in relative motion with the N S-spins, the REDOR fraction is given by[35]

$$\Delta S = 1 - \frac{1}{8\pi^2}\int d\Omega \prod_{i=1}^{N}\cos_i\left[\sum_{j=1}^{n}\frac{4\sqrt{2}}{n}\nu_D{}^j N_c T_R \sin(2\beta^j)\sin(\alpha^j)\right] \quad (9)$$

There is one cosine term for each of the N S-spins and n is the number of steps that the S-spin moves through in its trajectory in some time interval.

For the 5.8 ppm ^{1}H{^{31}P} REDOR NMR experiments, Figure 9a shows the experimental ΔS as well as the best theoretical ΔS curves calculated for a single, static ^{1}H−^{31}P spin pair, a static ^{1}H spin coupled to two ^{31}P spins, and a single ^{1}H spin in relative motion to two ^{31}P spins. The relative motion was modeled assuming that the lone proton hops between two sites so that $n = 2$ in eq 9. The models where the ^{1}H is spin coupled to two ^{31}P spins with ^{1}H−^{31}P internuclear distances of 580 and 620 pm describes the experimental ^{1}H{^{31}P} REDOR NMR data well. In addition, the two ^{1}H−^{31}P internuclear vectors were found to lie along the ^{31}P−^{31}P internuclear vector indicating that the lone proton with a 5.8 ppm chemical shift resides on an edge of the unit cell. Hence, the sum of the two ^{1}H−^{31}P internuclear distances is constrained to be equal to the unit cell parameter $a = 1197$ pm as determined by XRD. The sum of the two ^{1}H−^{31}P internuclear vectors from REDOR NMR is 1200 pm, which agrees well with the XRD result. Because of the scatter in the experimental data points, all three models give adequate fits to the experimental data. Thus, whether the proton is static or hopping between the two sites or whether the lone

proton is coupled to one or two phosphorus atoms cannot be determined here.

The 2.7 ppm or water molecule proton $^{1}H\{^{31}P\}$ REDOR NMR results along with the calculated REDOR curves for three models are shown in Figure 9b. The models considered are one static $^{1}H-^{31}P$ dipolar coupling, static water molecule protons coupled to two ^{31}P spins and water molecule protons in relative motion to two ^{31}P spins. The motion of the water molecule protons was modeled assuming that the water molecule rotates about its C_2 symmetry axis, that is, $n = 2$ in eq 9. For ease in computation in the latter two models, the two protons of the water molecule and the two phosphorus nuclei were constrained to lie in the same plane. In this case, the motional model with $^{1}H-^{31}P$ internuclear distances of 580 and 690 pm and an angle of 140° between the two $^{1}H-^{31}P$ internuclear vectors gives the best agreement with the experimental results. This is consistent with the conclusion reached on the basis of the variable temperature ^{1}H NS NMR experiments where rotational motion was occurring. In addition, a simple trigonometric calculation using the theoretical REDOR parameters yields an interphosphorus distance of 1194 pm, in very good agreement with XRD result of $a = 1197$ pm.

Interpretation of the $^{31}P\{^{1}H\}$ REDOR NMR experiment is not as straightforward as that for the $^{1}H\{^{31}P\}$ REDOR NMR experiment because the number of possible $^{31}P-^{1}H$ couplings is potentially very large. However, some preliminary observations help to partially solve the structure. The $^{31}P\{^{1}H\}$ SEDOR NMR experiment shows that all ^{31}P nuclei are coupled to protons in the limiting hydrated form of HNaPW. The ICP results show that there are on average only 0.5 lone protons per unit cell. This result, used in combination with the relative intensities of Table 1, indicate that there are about four water molecules per unit cell. Table 4 shows that about 90% of the ^{31}P intensity contribution comes from the resonance lines with chemical shifts of −15.2 and −15.4 ppm indicating that these two phosphorus sites comprise the bulk of the phosphorus sites in the limiting hydrated form of HNaPW. While these considerations reduce the possible number of structures, the discussion that follows considers only the very simplest of structures. The structures proposed are meant to indicate the types of structures that *may* be present and should not be considered definitive.

Comparison of the experimental $^{31}P\{^{1}H\}$ REDOR fraction for the −15.4 and −15.2 ppm ^{31}P peaks, Figure 10a and 10b, respectively, shows that the $^{31}P\{^{1}H\}$ REDOR fraction for the −15.2 ppm peak approaches a value of 1 for shorter times than that of the −15.4 ppm resonance line. Theoretical $^{31}P\{^{1}H\}$ REDOR calculations (not shown) indicate that lone protons coupled to ^{31}P cause the ^{31}P signal to dephase more rapidly than water molecule protons coupled to ^{31}P. For example, when one of the water molecules in a two, three, or four water molecule $^{31}P\{^{1}H\}$ REDOR simulation is replaced by a lone proton, the $^{31}P\{^{1}H\}$ REDOR fraction is larger for shorter values of N_cT_r than for the cases where only water molecules are included. Thus, the −15.2 ppm ^{31}P resonance line is assigned to a structure where the Keggin anion is coupled to lone protons and the −15.4 ppm ^{31}P resonance line is assigned to Keggin anions that are not coupled to lone protons. These assignments and the relative intensities of Table 4 imply that two lone protons are coupled to the phosphorus site with a chemical shift of −15.2 ppm.

Figure 10a shows experimental and theoretical $^{31}P\{^{1}H\}$ REDOR NMR curves for the −15.4 ppm ^{31}P resonance line coupled to both three and four rotating water molecules. On the basis of the $^{1}H\{^{31}P\}$ REDOR NMR results for the water

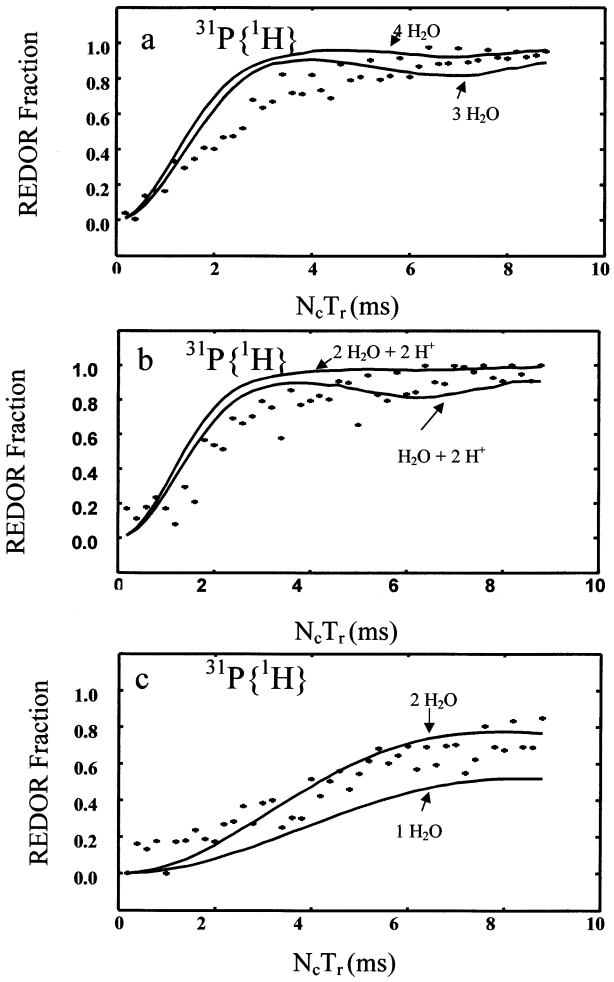

Figure 10. Plot of $^{31}P\{^{1}H\}$ REDOR fraction versus N_cT_r at $T = 310$ K and 10.0 kHz MAS. (a) −15.4 ppm ^{31}P peak, (b) −15.2 ppm ^{31}P peak, and (c) −15.0 ppm ^{31}P peak.

SCHEME 1

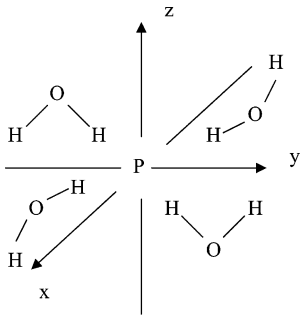

molecule resonance line, dipolar couplings of 150 and 250 Hz were used for the two protons of each of the three or four water molecules used in the theoretical calculation of Figure 10a. Scheme 1 depicts the configuration of the four water molecules. One pair of water molecules lies in the *yz* plane, one above and one below the *xy* plane. The second pair of water molecules lies in the *xz* plane with one above and one below the *xy* plane. The three water molecule configuration is obtained by removing one water molecule from the structure shown in Scheme 1. Both the three and four water molecule theoretical $^{31}P\{^{1}H\}$ REDOR curves agree fairly well with the experimental result. The fit for both models is rather poor for $N_cT_r = 2-5$ ms suggesting that the theoretical models may be too simple and that water molecule motions in addition to rotation may be important.

SCHEME 2

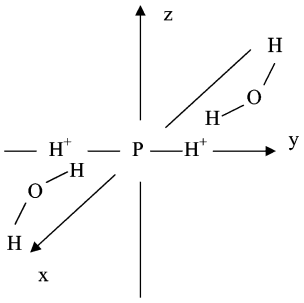

SCHEME 3

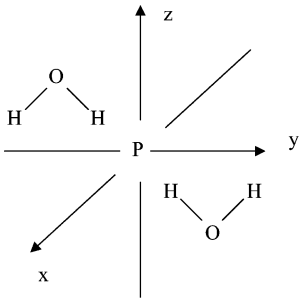

Figure 10b shows experimental and theoretical $^{31}P\{^1H\}$ REDOR NMR curves for the −15.2 ppm ^{31}P resonance line. Both theoretical models correspond to ^{31}P coupled to two hopping lone protons with one having two rotating water molecules (Scheme 2) and the second having one rotating water molecule (Scheme 2 with one water molecule removed). The lone protons lie on the $+y$ and $-y$ axes. On the basis of the $^1H\{^{31}P\}$ REDOR NMR results for the water molecule proton resonance line, dipolar couplings of 150 and 250 Hz were used for the two protons of each water molecule. On the basis of the $^1H\{^{31}P\}$ REDOR NMR results for the lone proton resonance line, dipolar couplings of 210 and 250 Hz were used for the two sites that the lone proton hops between. The configuration of the water molecules in Scheme 2 is similar to that described above for Scheme 1. The 2 H_2O + 2 H^+ and H_2O + 2 H^+ models both provide good fits of the experimental data.

Figure 10c shows experimental and theoretical $^{31}P\{^1H\}$ REDOR NMR curves for the −15.0 ppm ^{31}P resonance line. The theoretical models correspond to ^{31}P coupled to one or two rotating water molecules. The configuration of the two water molecule model is shown in Scheme 3 and is similar to that described above in Scheme 1. Removing one of the water molecules from Scheme 3 gives the configuration for a one water molecule model. The two H_2O model gives a good fit to the experimental data.

On the basis of the 4 H_2O and 2 H_2O + 2 H^+ models for fits of the −15.4 ppm and −15.2 ppm ^{31}P peaks, respectively, of the $^{31}P\{^1H\}$ REDOR NMR data, the total theoretical number of water molecules per phosphorus atom in the limiting hydrated form of HNaPW is 3.4. This value agrees reasonably well with the experimental value of 4.0 ± 0.4 obtained from ICP analysis and 4 measured using thermal gravimetric analysis.

The phosphorus-proton internuclear distances calculated from the REDOR experiments can be used in combination with the phosphorus−oxygen internuclear distances determined from neutron diffraction analysis of HPW[15] to locate the position of the protons in the limiting hydrated form of HNaPW. Neutron diffraction[15] yields P−O internuclear distances of 335, 393, and 523 pm for P−O_e, P−O_c, and P−O_t nuclear pairs, respectively. Results of the REDOR experiments show that each P−H distance is greater than 523 pm. Thus, both the lone proton and the water molecule protons reside in and are part of the so-called secondary structure of the limiting hydrated form of HNaPW.

Infrared Spectroscopy. Figure 11 shows the IR spectrum of HNaPW close to its limiting hydrated form. The structural assignments discussed below are summarized in Table 5. In the fully hydrated salt, very broad bands due to the large continuum of disordered water in motion define the IR spectrum.[70] Residual bands from incomplete drying of HNaPW are seen as broad features assigned to $\nu(O_wH)$, $\delta(O_wH)$, and $\gamma(O_wH)$ centered at 3450, 1700, and 762 cm^{-1}. The IR spectrum of HNaPW is surprisingly sharp indicating a well-ordered static structure on the infrared time scale. Of the three bands assigned to ν(OH), two are water, $\nu(O_wH^+)$, at 3592 and 3536 cm^{-1} and one is from the lone proton binding to the terminal oxygen atoms, O_t, of the Keggin structure, $\nu(O_tH)$, 3254 cm^{-1}. The REDOR experiments suggest that all the hydrogen atoms are associated with O_t atoms of the Keggin anions. Thus, from IR/crystallographic correlations[71] the lone proton asymmetrically bridges

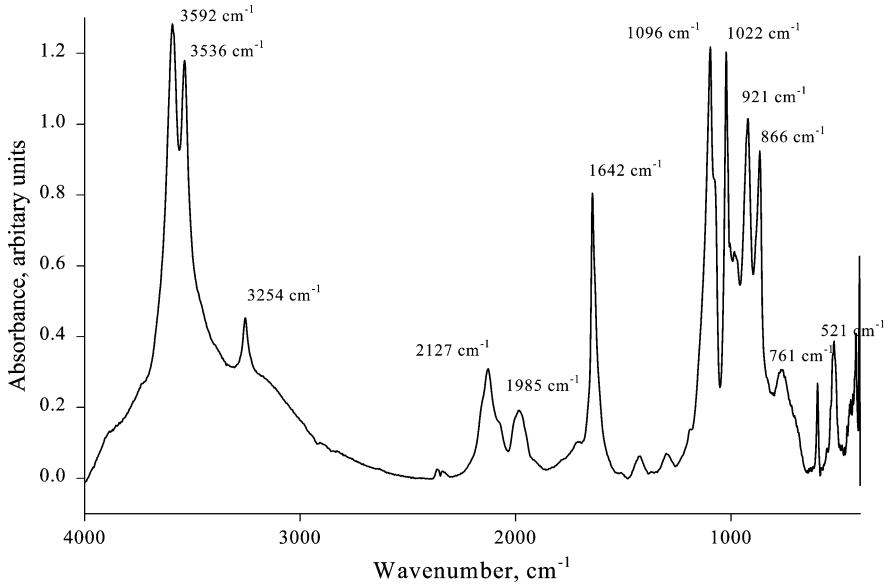

Figure 11. DRIFTS spectrum of the limiting hydrated form of HNaPW.

TABLE 5: Infrared Assignments for the Limiting Hydrated Form of HNa_2PW

band	wavenumber (cm^{-1})	strength/comment[a]
$\nu(O_wH^+)$	3592	S
	3536	S
$\nu(O_tH)$	3254	M
ν (ONa)	2127	MC
	1984	MC
$\delta(O_wH)$	1643	S
ν (OP)	1096	S
$\nu(O_tW)$	1072	M
	1042	W
	1022	S
	1000	M
	983	M
	970	M
$\nu(O_cW)$	938	M
	920	S
$\nu(O_eW)$	884	M
	865	S
$\gamma(O_tH^+)$	597	M
	521	M
$\gamma(O_wH^+)$	419	M

[a] S, strong; M, medium;, W, weak; C, complex.

four O_t atoms with O_t....O_t distances of 288 and 291 pm and the hydrogen-bonded water molecule is bound to two O_t atoms with an O_t....O_w distance of 271 pm.

The complex bands at 2127 and 1984 cm^{-1} are tentatively assigned to ν(ONa) of the interaction of the sodium cation with the Keggin anion O_t, corner and edge oxygens, O_c and O_e. Only one $\delta(O_wH)$ band is observed at 1643 cm^{-1}, which is assigned to the water molecule, as the bending modes of hydrogen-bonded molecules are often mixed with other vibrational modes. In this system, it seems that any bending modes of the lone proton are mixed modes and might not be as strong or obvious as those of the pure water-bending mode.

The Keggin anion bands provide useful information about the interaction of the Keggin anion with the secondary structure. With the exception of the single ν(OP) at 1096 cm^{-1}, all the other Keggin anion bands are unusually complex. The whole Keggin anion region of the spectrum was deconvoluted to give the bands in Table 5. The terminal oxygen atoms are postulated to bind as follows: four in two pairs to the lone proton, two asymmetrically to axial positions of the octahedral sodium cation, two symmetrically to the water molecule, and four as free unbound O_t. This bonding pattern of the terminal oxygen atoms gives rise to six bands: 1072, 1042, 1022, 1000, 983, and 970 cm^{-1} with the highest wavenumber band 1072 cm^{-1} assigned to the free $\nu(O_tW)$. Both the O_c and O_e of the Keggin anion are either free or are bound to the two sodium cations equatorially, giving rise to $\nu(O_cW)$ and $\nu(O_eW)$ bands at 938, 920, 884, and 865 cm^{-1}. Three distinct bands are observed at low wavenumber, 597, 521, and 419 cm^{-1}, which are pure bands, and correlate to the ν(OH)[71] and are therefore assigned to the two $\gamma(O_tH^+)$ and $\gamma(O_wH)$, respectively.

Conclusions

The isolated pair of protons in the limiting hydrated form of HNaPW are protons of a water molecule. Translational diffusion of the protons in the limiting hydrated form of HNaPW is significant above 293 K. The two unique sodium sites in the limiting hydrated form of HNaPW correspond to a sodium coordination number of six. The total theoretical number of water molecules per phosphorus atom in the limiting hydrated form of HNaPW is 3.4.

Acknowledgment. This research was funded in part by both DOE award DE-FC36-01CH11088 and NSF award CTS-9512228. We thank James L. Horan for performing the ICP analysis.

Supporting Information Available: Figures showing ^1H, ^{23}Na, and ^{31}P NMR spectra of the limiting hydrated form of HNaPW at various temperatures, a plot of the apparent dipolar coupling, and ^{23}Na and ^{31}P SEDOR fractions. A table containing diffusion coefficients and r_{max}/d values. This material is available free of charge via the Internet at http://pubs.acs.org.

References and Notes

(1) Savadogo, O. *J. New Mater. Electrochem. Syst.* **1998**, *1*, 47.
(2) Steele, B. C. H.; Heinzel, A. *Nature* **2001**, *414*, 345.
(3) Kreuer, K. D. *Chem. Mater*. **1996**, *8*, 610−641.
(4) Gottesfeld, S.; Zawodzinski, T. A. In *Advances in Electrochemical Science and Engineering*; Alkire, R. C., Gerischer, H., Kolb, D. M., Tobias, C. W., Eds.; Wiley/VCH: New York, 1997; p 197.
(5) Malhotra, S.; Datta, R. *J. Electrochem. Soc.* **1997**, *144*, L23.
(6) Staiti, P.; Aricò, A. S.; Baglio, V.; Lufrano, F.; Passalacqua, E.; Antonucci, V. *Solid State Ionics* **2001**, *145*, 101−107.
(7) Staiti, P.; Minutoli, M.; Hocevar, S. *J. Power Sources* **2000**, *90*, 231−235.
(8) Wu, Q.; Tao, S.; Lin, H.; Meng, G. *Mater. Chem. Phys.* **2000**, *64*, 25−28.
(9) Zaidi, S. M. J.; Mikhailenk, S. D.; Robertson, G. P.; Guiver, M. D.; Kaliaguine, S. *J. Membr. Sci*. **2000**, *173*, 17−34.
(10) Staiti, P. *Mater. Lett.* **2001**, *47*, 241−246.
(11) Park, Y.-I.; Nagai, M. *J. Electrochem Soc.* **2001**, *148*, A616.
(12) Lorrenčič Stanger, U.; Grošelj, N.; Orel, B.; Schmitz, A.; Colomban, Ph. *Solid State Ionics* **2001**, *145*, 109−118.
(13) Spirlet, M.-R.; Busing, W. R. *Acta Crystallogr*. **1978**, *B34*, 907−910.
(14) d'Amour, H.; Allman, R. *Z. Kristallogr*. **1976**, *143*, 1−13.
(15) Brown, G. M.; Spirlet, M.-R.; Busing, W. R.; Levy, H. A. *Acta Crystallogr*. **1977**, *B33*, 1038−1046.
(16) Strandberg, R. *Acta Chem. Scand. Series A, Phys. Inorg. Chem.* **1975**, *A29*, 359−364.
(17) Allmann, R. *Acta Chem. Scand. Series A, Phys. Inorg. Chem.* **1976**, *A30*, 152.
(18) Ukshe, E. A.; Leonova, L. S.; Korsteleva, A. I. *Solid State Ionics* **1989**, *36*, 219−223.
(19) Pressman, H. A.; Slade, R. C. T. *Chem. Phys. Lett*. **1988**, *151*, 354−361.
(20) Slade, R. C. T.; Barker, J.; Pressman, H. A.; Strange, J. H. *Solid State Ionics* **1988**, *28*−*30*, 594−600.
(21) Filowitz, M.; Klemperer, W. G.; Messerle, L.; Shum, W. *J. Am. Chem. Soc*. **1976**, *98*, 2345−2346.
(22) Filowitz, M.; Ho, R. K. C.; Klemperer, W. G.; Shum, W. *Inorg. Chem.* **1979**, *18*, 93−103.
(23) Uchida, S.; Inumaru, K.; Misono, M. *J. Phys. Chem. B* **2000**, *104*, 8108−8115.
(24) Chidichimo, G.; Golemme, A.; Imbardelli, D.; Santoro, E. *J. Phys. Chem*. **1990**, *94*, 6826−6830.
(25) Chidichimo, G.; Golemme, A.; Imbardelli, D.; Iannibello, A. *J. Chem. Soc., Faraday Trans*. **1992**, *88*, 483−487.
(26) Rocchiccioli-Deltcheff, C.; Fournier, M.; Franck, R.; Thouvenot, R. *Inorg. Chem.* **1983**, *22*, 207.
(27) Essayem, N.; Holmqvist, A.; Gayraud, P., Y.; Vedrine, J. C.; Ben Traarit, Y. *J. Catal.* **2001**, *197*, 273−280.
(28) Mioc, U.; Colomban, P.; Novak, A. *J. Mol. Struct.* **1990**, *218*, 123−128.
(29) Highfield, J., G.; Moffat, J. B. *J. Catal.* **1984**, *88*, 177−187.
(30) Kanda, Y.; Lee, K. Y.; Nakata, S.; Asaoka, S.; Misono, M. *Chem. Lett*. **1988**, 139−142.
(31) Uchida, S.; Inumaru, K.; Dereppe, J. M.; Misono, M. *Chem. Lett*. **1998**, 643−644.
(32) Gullion, T.; Schaefer, J. *J. Magn. Reson*. **1989**, *81*, 196−200.
(33) Pan, P.; Gullion, T.; Schaefer, J. *J. Magn. Reson.* **1990**, *90*, 330−340.
(34) Schmidt, A.; Kowalewski, T.; Schaefer, J. *Macromolecules* **1993**, *26*, 1729−1733.
(35) Goetz, J. M.; Schaefer, J. *J. Magn. Reson*. **1997**, *127*, 147−154.
(36) Wang, P.-K.; Slichter, C. P. *Phys. Rev. Lett*. **1984**, *53*, 82−85.
(37) Wang, P.-K.; Ansermet, J.-P.; Slichter, C. P. *Phys. Rev. Lett*. **1985**, *55*, 2731−2734.
(38) Zax, D. B.; Klug, C. A.; Slichter, C. P.; Sinfelt, J. H. *J. Phys. Chem.* **1989**, *89*, 5009−5012.

(39) Wang, P.-K.; Slichter, C. P.; Sinfelt, J. H. *J. Phys. Chem*. **1990**, *94*, 1154−1157.
(40) Nevzorov, A. A.; Freed, J. H. *J. Chem. Phys*. **2000**, *112*, 1413−1424.
(41) Nevzorov, A. A.; Freed, J. H. *J. Chem. Phys*. **2000**, *112*, 1425−1443.
(42) Cory, D. G.; Ritchey, W. M. *J. Magn. Reson*. **1988**, *80*, 128−132.
(43) Fukushima, E.; Roeder, S. B. W. *Experimental Pulse NMR. A Nuts and Bolts Approach*; Addison-Wesley: Reading, MA, 1981; pp 172−176.
(44) Fukushima, E.; Roeder, S. B. W. *Experimental Pulse NMR. A Nuts and Bolts Approach*; Addison-Wesley: Reading, MA, 1981; pp 106−112.
(45) van Geet, A. L. *Anal. Chem*. **1970**, *42*, 679−680.
(46) van Geet, A. L. *Anal. Chem*. **1968**, *40*, 2227−2229.
(47) Bielecki, A.; Burum, D. P. *J. Magn. Reson. A* **1995**, *116*, 215−220.
(48) Holland, T. J. B.; Redfern, S. A. T. *Mineral. Magn*. **1997**, *61*, 65−77.
(49) The MathWorks, Inc., 24 Prime Park Way, Natick, MA 01760.
(50) Siderer, Y.; Luz, Z. *J. Magn. Reson*. **1980**, *37*, 449−463.
(51) Zilm, K. W.; Grant, D. M. *J. Am. Chem. Soc*. **1981**, *103*, 2913−2922.
(52) Andrew, E. R.; Bersohn, R. *J. Chem. Phys*. **1950**, *18*, 159−161.
(53) Taylor, P. C.; Baugher, J. F.; Kriz, H. M. *Chem. Rev*. **1975**, *75*, 203−240.
(54) Carrington, A.; McLachlan, A. D. *Introduction to Magnetic Resonance*; Harper and Row: New York, 1967; pp 34−36.
(55) Schmidt-Rohr, K.; Spiess, H. W. *Multidimensional Solid-State NMR and Polymers*; Academic Press: New York, 1994; pp 130−132.
(56) Richards, R. E.; Smith, J. A. S. *J. Chem. Soc., Faraday Trans.* **1951**, *47*, 1261−1274.
(57) Pake, G. E. *J. Chem. Phys*. **1948**, *16*, 327−336.
(58) Schmidt-Rohr, K.; Spiess, H. W. *Multidimensional Solid-State NMR and Polymers*; Academic Press: New York, 1994; pp 28−32.
(59) Burum, D. P.; Rhim, W. K. *J. Chem. Phys*. **1979**, *70*, 3553−3554.
(60) Rhim, W. K.; Burum, D. P.; Elleman, D. D. *J. Chem. Phys*. **1979**, *71*, 3139−3141.
(61) Schmidt-Rohr, K.; Spiess, H. W. *Multidimensional Solid-State NMR and Polymers*; Academic Press: New York, 1994; pp 25−26.
(62) Eisenberg, D.; Kauzmann, W. *The Structure and Properties of Water*; Oxford University Press: New York, 1969; p 145.
(63) Günther, H. *NMR Spectroscopy*, 2nd ed.; John Wiley and Sons: New York, 1995; pp 336−341.
(64) Pople, J. A.; Schneider, W. G.; Bernstein, H. J. *High-resolution Nuclear Magnetic Resonance*; McGraw-Hill Book Company: New York, 1959; p 221.
(65) Dec, S. F.; Maciel, G. E. *J. Magn. Reson*. **1990**, *87*, 153−159.
(66) Dec, S. F.; Fitzgerald, J. J.; Maciel, G. E. *J. Am. Chem. Soc*. **1990**, *112*, 9069−9077.
(67) Bancroft, G. M.; Platt, R. H. *Adv. Inorg. Chem. Radiochem*. **1972**, *15*, 59−258.
(68) Kao, H.-M.; Stefanescu, A. D.; Wooley, K. L.; Schaefer, J. *Macromolecules* **2000**, *33*, 6214−6216.
(69) $d\Omega = d\phi \sin\theta\, d\theta\, d\psi$ where ϕ, θ, ψ are the Euler angles and $\sin 2\beta^i \sin\alpha^i = 2\{[\sin\theta\cos\phi]\mathbf{x}(i) + [\sin\theta\sin\phi]\mathbf{y}(i) + [\cos\theta]\mathbf{z}(i)\}\{[-\cos\psi\sin\phi - \cos\theta\cos\phi\sin\psi]\mathbf{x}(i) + [\cos\psi\cos\phi - \cos\theta\sin\phi\sin\psi]\mathbf{y}(i) + [\sin\psi\sin\theta]\mathbf{z}(i)\}$ and $\mathbf{x}(i)$, $\mathbf{y}(i)$, $\mathbf{z}(i)$ are unit vectors describing the orientation of each I−S spin pair internuclear vector. See ref 35 for a detailed derivation.
(70) Puze, C.; Bordigo, S.; Zecchinu, A. *Langmuir* **2000**, *16*, 8139.
(71) Novak, A. *Struct. Bonding* **1974**, *18*, 177−216.